Leaky wave excitation on three-dimensional via-fed printed interconnects

George W. Hanson

Department of Electrical Engineering, University of Wisconsin-Milwaukee, Milwaukee, Wisconsin, USA

Alexander B. Yakovlev and W. Elliott Hutchcraft

Department of Electrical Engineering, University of Mississippi, University, Mississippi, USA

Received 1 September 2004; revised 15 March 2005; accepted 2 May 2005; published 14 September 2005.

[1] Leaky wave excitation on three-dimensional, via-fed single and coupled microstrip interconnects is studied. Closed-form asymptotic expressions for the fields associated with the interconnect are derived and are applied in the traveling/standing wave and leaky wave regimes, both of which lead to radiation. The leaky wave beam angle is found to correspond to the usual two-dimensional ray optics leakage angle for long interconnects, as expected, and depends on interconnect length, spacing, and excitation for shorter interconnects. Comparisons with full-wave results are shown for the case of via-fed coupled interconnects.

Citation: Hanson, G. W., A. B. Yakovlev, and W. E. Hutchcraft (2005), Leaky wave excitation on three-dimensional via-fed printed interconnects, *Radio Sci.*, *40*, RS6S08, doi:10.1029/2004RS003168.

1. Introduction

[2] Leaky waves on printed-circuit transmission lines have recently received considerable attention. Radiation into space waves, surface waves, and both wave types have been investigated for a variety of two-dimensional microstrip-like lines, coplanar lines, and various printed transmission line modifications [*Michalski and Zheng*, 1989; *Shigesawa et al.*, 1991, 1995, 1996; *Carin and Das*, 1992; *Bagby et al.*, 1993; *Nghiem et al.*, 1995, 1996; *Yakovlev and Hanson*, 1997; *Nyquist et al.*, 1997]. Experience gained in the study of leaky wave open boundary waveguides has resulted in the development of novel microwave and millimeter wave devices and components, such as leaky wave couplers [*Niu et al.*, 1993] and leaky wave antennas, although many studies have concentrated on the potentially harmful effects of unintended crosstalk, coupling, and radiation due to leaky waves on integrated circuits.

[3] In many practical applications, circuit board and on-chip interconnects are constructed from finite sections of transmission lines. The possibility of leaky wave excitation on these three-dimensional interconnects has received relatively little attention [*Das*, 1996; *Carin et al.*, 1998], compared to two-dimensional structures, although semi-infinite source-excited lines have been somewhat more thoroughly studied [*Villegas et al.*, 1999; *Mesa et al.*, 1999, 2001; *Jackson et al.*, 2000; *Mesa and Jackson*, 2002; *Langston et al.*, 2003]. While it is clear that the simpler two-dimensional transmission line model can be used as a starting point for considering leaky waves on three-dimensional structures, the degree to which two-dimensional results predict three-dimensional phenomena is still an open question. For example, *Das* [1996] reported that the onset of leakage on certain three-dimensional transmission line structures seems to occur at a different point than that predicted by two-dimensional theory. Furthermore, in previous studies simplified excitations (generally, delta gaps) were considered, or the influence of the feed was ignored.

[4] In this paper we investigate three-dimensional microstrip interconnect geometries, with realistic excitations, and derive asymptotic closed-form expressions for the field radiated by such structures. The field along the air-dielectric interface is considered, since potential crosstalk with other devices may depend on the field at this interface. The results are compared to a full-wave, three-dimensional simulation in both the traveling/standing wave (TSW) regime (analogous to the bound regime on two-dimensional transmission lines; see section 3) and leaky wave (LW) regime, verifying the developed expressions. It is shown that in the leaky wave regime the angle of leakage on a three-dimensional interconnect corresponds with the usual two-dimensional ray optics result if the interconnect is sufficiently long, even for

0048-6604/05/2004RS003168$11.00

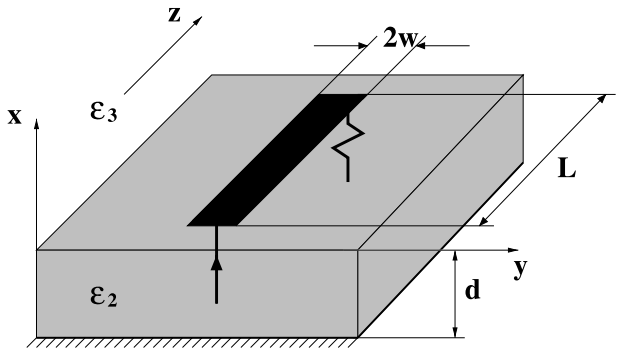

Figure 1. Three-dimensional via-fed interconnect structure.

coupled interconnects. For shorter interconnect strips, the influence of interconnect length, spacing, and of the via is important. This paper is a considerably expanded version of *Hanson et al.* [2004] and *Hanson and Yakovlev* [2004].

2. Formulation

[5] A three-dimensional microstrip interconnect, fed and terminated by cylindrical vias, is depicted in Figure 1 (notation associated with the grounded slab was chosen to be consistent with *Hanson* [2005]).

[6] For the laterally infinite grounded dielectric slab, the Hertzian potential dyadic Green's function can be written in eigenfunction form as [*Hanson*, 2005]

$$\begin{aligned}\mathbf{g}(\vec{\mathbf{r}},\vec{\mathbf{r}}') &= \mathbf{g}^d(\vec{\mathbf{r}},\vec{\mathbf{r}}') + \mathbf{g}^c(\vec{\mathbf{r}},\vec{\mathbf{r}}') \\ &= \sum_{\beta\beta=xx,yy,zz} \mathbf{D}^{\beta\beta} \cdot \int_{-\infty}^{\infty}\int_{-\infty}^{\infty} \left\{ \sum_{n_e=1}^{N_e} \frac{\mathbf{u}_{n_e}^{\beta\beta}(x)\,\overline{v}_{n_e,\beta\beta}(x')}{k_\rho^2 - \beta_{sw,n_e}^2} \right. \\ &+ \sum_{n_h=1}^{N_h} \frac{\mathbf{u}_{n_h}^{\beta\beta}(x)\,\overline{v}_{n_h,\beta\beta}(x')}{k_\rho^2 - \beta_{sw,n_h}^2} + \int_{-k_u^2}^{\infty} \frac{\mathbf{u}_{\xi_e}^{\beta\beta}(x)\,\overline{v}_{\xi_e,\beta\beta}(x')}{k_\rho^2 + \xi_e} d\xi_e \\ &+ \left. \int_{-k_u^2}^{\infty} \frac{\mathbf{u}_{\xi_h}^{\beta\beta}(x)\,\overline{v}_{\xi_h,\beta\beta}(x')}{k_\rho^2 + \xi_h} d\xi_h \right\} \frac{e^{jk_y(y-y')}}{2\pi} \frac{e^{jk_z(z-z')}}{2\pi} dk_y dk_z, \end{aligned} \tag{1}$$

where the overbar indicates complex conjugation, n_e and n_h indicate E (transverse magnetic (TM)) and H (transverse electric (TE)) discrete surface wave modes, respectively (and similarly for the TM and TE continuous spectrum over ξ_e and ξ_h), N_e and N_h are the number of above cutoff TM and TE surface waves, respectively, $k_\rho^2 = k_y^2 + k_z^2$ is the radial wave number, $\beta_{sw,n}$ is the propagation constant of the nth surface waveguided by the grounded dielectric slab, and $\mathbf{D}^{xx} = \hat{\mathbf{x}}\hat{\mathbf{x}}$, $\mathbf{D}^{\alpha\alpha} = \hat{\mathbf{x}}\,\hat{\mathbf{x}}\frac{\partial}{\partial\alpha} + \hat{\boldsymbol{\alpha}}\hat{\boldsymbol{\alpha}}$ for $\alpha = y, z$. The superscripts d and c indicate the discrete and continuous contributions to the Green's dyadic, respectively. The eigenfunctions $\mathbf{u}$ and adjoint eigenfunctions $\mathbf{v}$ are defined by *Hanson* [2005]. An alternative form for the Green's function is

$$\begin{aligned}\mathbf{g}(\vec{\mathbf{r}},\vec{\mathbf{r}}') &= \mathbf{g}^d(\vec{\mathbf{r}},\vec{\mathbf{r}}') + \mathbf{g}^c(\vec{\mathbf{r}},\vec{\mathbf{r}}') \\ &= \sum_{\beta\beta=xx,yy,zz} \mathbf{D}^{\beta\beta} \cdot \left\{ \sum_{n_e=1}^{N_e} \mathbf{u}_{n_e}^{\beta\beta}(x)\,\overline{v}_{n_e,\beta\beta}(x') H_0^{(2)}\left(\beta_{sw,n_e}\rho\right) \right. \\ &+ \sum_{n_h=1}^{N_h} \mathbf{u}_{n_h}^{\beta\beta}(x)\,\overline{v}_{n_h,\beta\beta}(x') H_0^{(2)}\left(\beta_{sw,n_h}\rho\right) \\ &+ \int_0^{\infty} \mathbf{u}_{\varsigma_e}^{\beta\beta}(x)\,\overline{v}_{\varsigma_e,\beta\beta}(x') H_0^{(2)}\left(\sqrt{k_u^2 - \kappa_e}\rho\right) d\kappa_e \\ &+ \left. \int_0^{\infty} \mathbf{u}_{\varsigma_h}^{\beta\beta}(x)\,\overline{v}_{\varsigma_h,\beta\beta}(x') H_0^{(2)}\left(\sqrt{k_u^2 - \kappa_h}\rho\right) d\kappa_h \right\} \frac{1}{4j}, \end{aligned} \tag{2}$$

where $\rho = ((y - y')^2 + (z - z')^2)^{1/2}$. The pure spectral form (1) will be used to obtain the field due to horizontal currents on the microstrip interconnect, whereas the modal form (2) will be used to obtain the field from the vertical via feeds.

[7] The electric and magnetic fields are

$$\begin{aligned}\vec{\mathbf{E}}(\vec{\mathbf{r}}) &= \left(k^2(x) + \boldsymbol{\nabla}\boldsymbol{\nabla}\cdot\right)\vec{\boldsymbol{\pi}}(\vec{\mathbf{r}}) \\ \vec{\mathbf{H}}(\vec{\mathbf{r}}) &= j\omega\varepsilon(x)\boldsymbol{\nabla}\times\vec{\boldsymbol{\pi}}(\vec{\mathbf{r}}), \end{aligned} \tag{3}$$

where

$$\begin{aligned}\vec{\boldsymbol{\pi}}(\vec{\mathbf{r}}) &= \int_\Omega \left(\mathbf{g}^d(\vec{\mathbf{r}},\vec{\mathbf{r}}') + \mathbf{g}^c(\vec{\mathbf{r}},\vec{\mathbf{r}}')\right)\cdot\frac{\vec{\mathbf{J}}(\vec{\mathbf{r}}')}{j\omega\varepsilon(x')} d\Omega' \\ &= \vec{\boldsymbol{\pi}}^d(\vec{\mathbf{r}}) + \vec{\boldsymbol{\pi}}^c(\vec{\mathbf{r}}). \end{aligned} \tag{4}$$

[8] We will concentrate on the fields excited along the surface of the slab (at $x = 0$) for $\rho \gg 1$. In this case the continuous spectrum contribution $\mathbf{g}^c$ is very small compared to the discrete spectrum contribution $\mathbf{g}^d$. In particular, as shown in the following, the discrete contribution varies as $1/\sqrt{\rho}$. As shown in Appendix A, the continuous spectrum contribution varies as $1/\rho^2$. Therefore the discrete contribution is dominant for $\rho \gg 1$, and so in what follows we will consider only the discrete contribution to $\mathbf{g}^d$, leading to $\vec{\boldsymbol{\pi}}^d$.

2.1. Field Due to a Vertical Via Source

[9] We consider a microstrip interconnect fed by a vertical cylindrical via. The via is infinitely thin, and carries the current $\vec{\mathbf{J}} = \hat{\mathbf{x}}\,J_x$,

$$J_x(x,y,z) = I_0^p f(x)\delta(y - y_0)\delta(z - z_0), \tag{5}$$

for $x \in [-d, 0]$, where $f(x)$ is a given current profile. The total current on the via at $x = 0$ (the via-strip intersection) is

$$I_p = \int J_x(0,y,z)dS = I_0^p f(0). \tag{6}$$

We will assume $f(0) = 1$. The resulting potential is, from (4),

$$\vec{\pi}^d(\vec{r}) = \hat{x}\pi_x^d(x,y,z)$$

$$\pi_x^d(x,y,z) = \frac{I_0^p}{j\omega\varepsilon_2}\int_{x=-d}^{0} g_{xx}^d(x,y,z,x',y_0,z_0)f(x')dx', \quad (7)$$

where

$$g_{xx}^d = \frac{1}{4j}\sum_{n_e=1}^{N_e} u_{n_e,xx}(x)\,\overline{v}_{n_e,xx}(x')H_0^{(2)}\left(\beta_{sw,n_e}\rho_p\right) \quad (8)$$

(since a vertical current will only excite TM modes) with $\rho_p = ((y - y_0)^2 + (z - z_0)^2)^{1/2}$. Upon defining

$$h\left(\beta_{sw,n_e}\right) = \int_{x=-d}^{0} \overline{v}_{n_e,xx}(x')f(x')dx', \quad (9)$$

assuming $\beta_{sw,n_e}\rho_p \gg 1$ and approximating the Hankel function using its large-argument form, and using the eigenfunctions (56) and (63)–(64) of *Hanson* [2005], the electric field along the surface of the interface ($x = 0$) due to a via is obtained as

$$E_x^v = I_0^p\sum_{n_e=1}^{N_e} c_{x,n_e}^p\frac{e^{-j\beta_{sw,n_e}\rho_p}}{\sqrt{\rho_p}} \quad (10)$$

$$E_y^v = \frac{y - y_0}{\rho_p}I_0^p\sum_{n_e=1}^{N_e} c_{y,n_e}^p\frac{e^{-j\beta_{sw,n_e}\rho_p}}{\sqrt{\rho_p}} \quad (11)$$

$$E_z^v = \frac{z - z_0}{\rho_p}I_0^p\sum_{n_e=1}^{N_e} c_{z,n_e}^p\frac{e^{-j\beta_{sw,n_e}\rho_p}}{\sqrt{\rho_p}}, \quad (12)$$

where

$$c_{x,n_e}^p = C_{n_e}\frac{-\left(\beta_{sw,n_e}\right)^{3/2}h\left(\beta_{sw,n_e}\right)}{2\sqrt{2\pi}\omega\varepsilon_2}e^{j\pi/4} \quad (13)$$

$$c_{y,n_e}^p = C_{n_e}\frac{\left(\beta_{sw,n_e}\right)^{1/2}\sqrt{\beta_{sw,n_e}^2 - k_0^2}h\left(\beta_{sw,n_e}\right)}{2\sqrt{2\pi}\omega\varepsilon_2}e^{j3\pi/4} \quad (14)$$

$$= c_{z,n_e}^p, \quad (15)$$

and where

$$C_{n_e} = \left(\frac{-1 + e^{4\gamma_2 d} + 4\gamma_2 d e^{2\gamma_2 d}}{8N^2\gamma_2\cosh^2\gamma_2 d}e^{-2\gamma_2 d} + \left(\frac{1}{2\gamma_3}\right)\right)^{-1} \quad (16)$$

with $\gamma_j^2 = \beta_{sw,n}^2 - k_j^2$, $j = 2,3$.

[10] The fields maintained by the via current are completely determined subject to specifying the current profile $f(x)$ in (9), leading to $h(\beta_{sw,n_e})$. The via probes are not assumed to be matched to the interconnect, although reasonable choices for via radius and position are assumed. Since the substrate thickness d is not necessarily small compared to the wavelength in the dielectric, the assumption of constant current on the via is inappropriate. Because of the connection between the via and the strip at $x = 0$, and the via feed at $x = -d$, the current should be nonzero at the top and bottom of the via. At frequencies considered in this study (f = 6.5 GHz, 9 GHz, and 13 GHz; see section 3), d is approximately $\lambda/3$, $\lambda/2$, and $2\lambda/3$, respectively, where λ is the wavelength in the dielectric. Therefore it would be expected that the current would become zero somewhere along the via's length (e.g., a null point is forced to be near the midpoint of the via since the current is nonzero at the via ends). Full-wave simulation using Ansoft Ensemble verifies this fact, and so we assume the via current profile to be

$$f(x) = -\sin\left(\frac{\pi}{d}\left(x - \frac{d}{2}\right)\right) \quad (17)$$

for $x \in [-d, 0]$, which is the current on a traditional half-wave dipole shifted to put the null at the midpoint ($x = -d/2$) of the via and current maximums at the strip and feed connections, leading to

$$h\left(\beta_{sw,n_e}\right) = -d^2\gamma_2\frac{-1 + e^{2\gamma_2 d}}{\left(\gamma_2^2 d^2 + \pi^2\right)\left(e^{2\gamma_2 d} + 1\right)}. \quad (18)$$

[11] It was found that while the magnitude of the via field is somewhat insensitive to the choice of $f(x)$, the phase is not, and therefore the total field due to the sum of the interconnect strip current and via current is sensitive to the choice of via current profile. In particular, proper via modeling is important for correct prediction of the leakage angle for shorter interconnects, as described later.

2.2. Potential Due to a Traveling Wave Interconnect Current

[12] We now model the field due to the horizontal interconnect current. Assume a perfectly conducting printed strip at the air-dielectric interface $x = 0$ having length L (extending from $z = -L_1$ to $z = L_2$, $L_{1,2} \geq 0$, $L_2 - L_1 = L$), width $2w$, and centered at $y = y_0$. Assume the traveling wave strip current $\vec{J} = \hat{z}\,J_z$,

$$J_z = I_0^s\delta(x)\frac{1}{\sqrt{1 - \left(\frac{y - y_0}{w}\right)^2}}T_n\left(\frac{y - y_0}{w}\right)e^{-j\gamma_{ms}z}, \quad (19)$$

where γ_{ms} is a complex propagation constant and T_n is the nth order Chebyshev polynomial. For bound micro-

strip modes $\gamma_{ms} = \beta_{ms}$ is real valued and $\beta_{ms} > \beta_{sw}$. For leaky microstrip modes $\gamma_{ms} = \beta_{ms} - j\alpha$ is complex valued and $\beta_{ms} < \beta_{sw}$. The total current on the strip at the via-strip junction ($x = 0$, $z = z_0$) is

$$I_s = \int_{y_0-w}^{y_0+w} I_0^s \frac{1}{\sqrt{1-\left(\frac{y-y_0}{w}\right)^2}} T_n\left(\frac{y-y_0}{w}\right) e^{-j\gamma_{ms}z_0} dy = \begin{cases} I_0^s w\pi e^{-j\gamma_{ms}z_0}, & n = 0, \\ 0, & n \neq 0. \end{cases} \tag{20}$$

Since the current on the via at the via-strip junction (6) is assumed to be I_0^p, current continuity then demands that

$$I_0^s = \frac{I_0^p}{w\pi e^{-j\gamma_{ms}z_0}}. \tag{21}$$

[13] The associated potential is given by (4) where the necessary Green's components are

$$g_{xz}^d(\vec{\mathbf{r}}, \vec{\mathbf{r}}') = \frac{\partial}{\partial z} g_{xz}(\vec{\mathbf{r}}, \vec{\mathbf{r}}')$$
$$g_{zz}^d(\vec{\mathbf{r}}, \vec{\mathbf{r}}') = g_{zz}(\vec{\mathbf{r}}, \vec{\mathbf{r}}') \tag{22}$$

with

$$g_{\alpha z}(\vec{\mathbf{r}}, \vec{\mathbf{r}}') = \int_{-\infty}^{\infty}\int_{-\infty}^{\infty} \left\{ \sum_{n_e=1}^{N_e} \frac{u_{n_e,\alpha z}(x)\, \bar{v}_{n_e,zz}(x')}{k_y^2 + k_z^2 - \beta_{sw,n_e}^2} + \sum_{n_h=1}^{N_h} \frac{u_{n_h,\alpha z}(x)\, \bar{v}_{n_h,zz}(x')}{k_y^2 + k_z^2 - \beta_{sw,n_h}^2} \right\} \frac{e^{jk_y(y-y')}}{2\pi} \frac{e^{jk_z(z-z')}}{2\pi} dk_y dk_z \tag{23}$$

for $\alpha = x, z$. Defining

$$I_z(k_z) = \int_{-L_1}^{L_2} e^{-j\gamma_{ms}z'} e^{-jk_z z'} dz' = \frac{\left[e^{-j(\gamma_{ms}+k_z)L_2} - e^{j(\gamma_{ms}+k_z)L_1}\right]}{-j(\gamma_{ms}+k_z)} \tag{24}$$

and

$$I_y(k_y) = \int_{y_0-w}^{y_0+w} \frac{1}{\sqrt{1-\left(\frac{y'-y_0}{w}\right)^2}} T_n\left(\frac{y'-y_0}{w}\right) e^{-jk_y y'} dy' = w\pi J_n(k_y w) e^{-jk_y y_0} \{\Re(j^n) - j\Im(j^n)\}, \tag{25}$$

assuming $n = 0$ and that only the TM_0 mode is above cutoff (in which case $u_{zz}^{(3)} = 0$), and denoting $\beta_{sw} = \beta_{sw,0}$ leads to

$$\pi_x^d = \frac{I_0^s}{j\omega\varepsilon_0} \frac{1}{(2\pi)^2} u_{0,xz}(x)\, \bar{v}_{0,zz}(0) \frac{\partial}{\partial z} I(y, z, \beta_{sw})$$
$$\pi_z^d = 0, \tag{26}$$

where

$$I(y, z, \beta_{sw}) = \int_{-\infty}^{\infty}\int_{-\infty}^{\infty} \frac{I_y(k_y) I_z(k_z)}{k_y^2 + k_z^2 - \beta_{sw}^2} e^{jk_y y} e^{jk_z z} dk_y dk_z. \tag{27}$$

2.2.1. Asymptotic Evaluation of $I(y, z, \beta_{sw})$ by the Method of Steepest Descent

[14] To evaluate (27), note that

$$I(y, z, \beta_{sw}) = \int_{-\infty}^{\infty} \frac{\left[e^{-j(\gamma_{ms}+k_z)L_2} - e^{j(\gamma_{ms}+k_z)L_1}\right]}{-j(\gamma_{ms}+k_z)} e^{jk_z z} dk_z \times (w\pi) \int_{-\infty}^{\infty} \frac{J_0(k_y w) e^{-jk_y y_0}}{k_y^2 + k_z^2 - \beta_{sw}^2} e^{jk_y y} dk_y = 2\pi j w\pi \int_{-\infty}^{\infty} f(k_z) e^{jk_z z} e^{\pm j\sqrt{\beta_{sw}^2 - k_z^2}(y-y_0)} dk_z, \tag{28}$$

where the integral over k_y was evaluated using the residue theorem, and where

$$f(k_z) = \frac{\left[e^{-j(\gamma_{ms}+k_z)L_2} - e^{j(\gamma_{ms}+k_z)L_1}\right]}{-j(\gamma_{ms}+k_z)} \frac{J_0\left(\sqrt{\beta_{sw}^2 - k_z^2}\, w\right)}{\pm 2\sqrt{\beta_{sw}^2 - k_z^2}}. \tag{29}$$

With $\rho_s = ((y - y_0)^2 + z^2)^{1/2}$,

$$y - y_0 = \rho_s \cos\phi, \quad z = \rho_s \sin\phi$$
$$k_z = -\beta_{sw} \sin\theta, \quad dk_z = -\beta_{sw} \cos\theta d\theta \tag{30}$$

(28) becomes

$$I(y, z, \beta_{sw}) = \int_C g(\theta) e^{-j\beta_{sw}\rho_s \cos(\theta-\phi)} d\theta, \tag{31}$$

where

$$g(\theta) = -2\pi^2 j w \beta_{sw} f(-\beta_{sw} \sin\theta) \cos\theta. \tag{32}$$

The path of integration C is the path $k_z \in (-\infty, \infty)$ mapped to the steepest descent plane, as shown in Figure 2. In Figure 2, P indicates the mapping of the proper sheet in the k_z plane (where $\Re\sqrt{k_z^2 - \beta_{sw}^2} (\gtrless) 0$ for $y (\gtrless) 0$) into the steepest descent plane, and I indicates the mapping of the improper sheet.

[15] Deforming the integration contour C to the steepest descent contour SDC leads to

$$I(y, z, \beta_{sw}) = \int_{SDC} g(\theta) e^{-j\beta_{sw}\rho_s \cos(\theta-\phi)} d\theta + S = I_{SD} + S, \tag{33}$$

where S represents any singularities encountered in the deformation of the original integration contour C to the steepest descent contour SDC. Here we consider a finite length interconnect, and in Appendix B a semi-infinite interconnect (which leads to quite different results).

[16] Assuming $L_1, L_2 < \infty$, there are no singularities in the steepest descent plane. In particular, in the following we will consider the case $L_1 = L_2 = L/2$. In the integral (33) a stationary phase point occurs at $\theta_s = \phi$, leading to

$$I_{SD}(\phi,\rho) = \int_{SDC} g(\theta) e^{-j\beta_{sw}\rho\cos(\theta-\phi)} d\theta \tag{34}$$

$$\simeq c_{sd} f_{sd}(\beta_{sw},\phi)\frac{e^{-j\beta_{sw}\rho_s}}{\sqrt{\rho_s}}, \tag{35}$$

where

$$c_{sd} = -j\pi^2 wLe^{j\pi/4}\sqrt{\frac{2\pi}{\beta_{sw}}} \tag{36}$$

$$f_{sd}(\beta_{sw},\phi) = \frac{\sin\left((\gamma_{ms}-\beta_{sw}\sin\phi)\frac{L}{2}\right)}{(\gamma_{ms}-\beta_{sw}\sin\phi)\frac{L}{2}} J_0(w\beta_{sw}\cos\phi). \tag{37}$$

For a narrow strip ($w\beta_{sw} \ll 1$) the Bessel function does not contribute significantly to the angular dependence, and from (37) it can be seen that as L increases the width of the radiation beam will decrease.

2.2.2. Strip Fields

[17] The electric field along the interface due to a single strip interconnect is obtained from the potential (26), using (3), as

$$E_x^{ss} = c_{xx}\frac{\partial}{\partial z} I(y,z,\beta_{sw}) \tag{38}$$

$$E_y^{ss} = c_{yx}\frac{\partial^2}{\partial y\partial z} I(y,z,\beta_{sw}) \tag{39}$$

$$E_z^{ss} = c_{zx}\frac{\partial^2}{\partial z^2} I(y,z,\beta_{sw}), \tag{40}$$

where

$$c_{xx} = \frac{I_0^s}{j\omega\varepsilon_0}\frac{1}{(2\pi)^2}\beta_{sw}^2 u_{0,xz}(0)\,\overline{v}_{0,zz}(0) \tag{41}$$

$$c_{yx} = \frac{I_0^s}{j\omega\varepsilon_0}\frac{1}{(2\pi)^2}\frac{\partial}{\partial x}u_{0,xz}(x)\bigg|_{x=0}\overline{v}_{0,zz}(0) = c_{zx}. \tag{42}$$

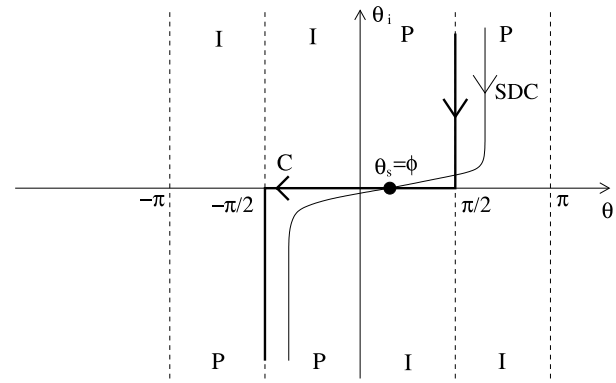

Figure 2. Steepest descent plane used for evaluation of (31).

Since

$$\frac{\partial}{\partial z} \leftrightarrow (jk_z) = -j\beta_{sw}\sin\phi \tag{43}$$

$$\frac{\partial}{\partial y} \leftrightarrow -j\sqrt{\beta_{sw}^2 - k_z^2} = -j\beta_{sw}\cos\phi, \tag{44}$$

we obtain

$$E_x^{ss} = E_{0x}\sin\phi f_{sd}(\beta_{sw},\phi)\frac{e^{-j\beta_{sw}\rho_s}}{\sqrt{\rho_s}} \tag{45}$$

$$E_y^{ss} = E_{0y}\sin\phi\cos\phi f_{sd}(\beta_{sw},\phi)\frac{e^{-j\beta_{sw}\rho_s}}{\sqrt{\rho_s}} \tag{46}$$

$$E_z^{ss} = E_{0z}\sin^2\phi f_{sd}(\beta_{sw},\phi)\frac{e^{-j\beta_{sw}\rho_s}}{\sqrt{\rho_s}}, \tag{47}$$

where, using (53), (54), (60), and (65) from *Hanson* [2005],

$$E_{0x} = j\beta_{sw}^3 E_0 \tag{48}$$

$$E_{0y} = -\beta_{sw}^2\sqrt{\beta_{sw}^2 - k_0^2}E_0 \tag{49}$$

$$E_{0z} = E_{0y} \tag{50}$$

$$E_0 = \frac{I_0^s C_0 wLe^{j\pi/4}}{4\omega\varepsilon_0}\sqrt{\frac{2\pi}{\beta_{sw}}} \times\left(\frac{(N^2-1)\cosh(\gamma_2 d)\sinh(\gamma_2 d)}{\gamma_2\cosh(\gamma_2 d)+\gamma_3\sinh(\gamma_2 d)}\right) \tag{51}$$

$$C_0 = \left(N^2\cosh(\gamma_2 d)\right)^{-1} C_{n0}, \tag{52}$$

and where C_{n0} is given by (16).

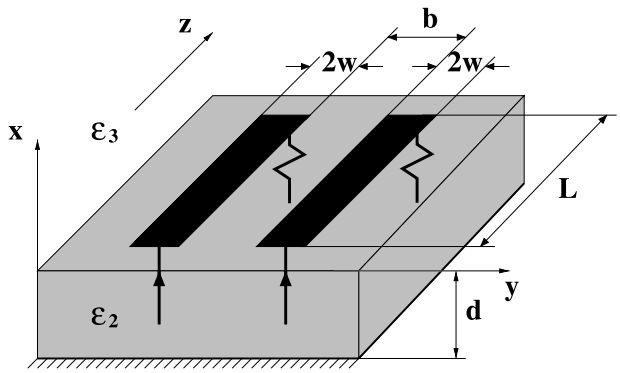

Figure 3. Three-dimensional via-fed coupled interconnect structure.

[18] The angular dependence of the field is given approximately by the angular dependence of the term f_{sd}, except if $\phi \simeq 0$, $\pi/2$. Defining $\psi = (\gamma_{ms} - \beta_{sw} \sin\phi)\frac{L}{2}$ and ignoring the Bessel function contribution in (37) we obtain

$$f_{sd}(\beta_{sw}, \phi) \simeq \frac{\sin(\psi)}{\psi}. \tag{53}$$

A beam maximum occurs when $\psi = 0$, leading to

$$\phi_{\max}^{LW} \simeq \phi_{\max}^{LW,2D} = \sin^{-1}\left(\frac{\beta_{ms}}{\beta_{sw}}\right), \tag{54}$$

which is the usual two-dimensional leakage angle for $\beta_{ms} < \beta_{sw}$ (we assume $\gamma_{ms} = \beta_{ms} - j\alpha \simeq \beta_{ms}$). For $\beta_{ms} > \beta_{sw}$ there is no real angle for leakage, although radiation maxima occur approximately when the numerator of (53) is unity, leading to

$$\phi_{\max}^{TSW} \simeq \sin^{-1}\left(\frac{\beta_{ms}}{\beta_{sw}} - (2n-1)\frac{\pi}{L\beta_{sw}}\right), \tag{55}$$

$n = 1, 2, 3, ..N_{Lobes}^{TSW}$, where

$$N_{Lobes}^{TSW} = \frac{L\beta_{ms}}{2\pi} \tag{56}$$

is the number of forward lobes in the range $0 \le \phi \le \pi/2$. More accurate angles can be obtained by replacing $(2n - 1)\ \pi$ in (55) with $2x_0$, where x_0 are the maxima of the $\sin(x)/x$ function (x_0 = 4.493, 7.725, 10.904, etc.). Note that (56) is a generalization of the formula for the number of lobes of a traveling wave antenna in free space, $N = L/\lambda$ [*Stutzman and Thiele*, 1998]. Pattern nulls occur when $\sin\psi = 0$, leading to

$$\phi_{null}^{TSW} \simeq \sin^{-1}\left(\frac{\beta_{ms}}{\beta_{sw}} \mp 2n\frac{\pi}{L\beta_{sw}}\right) \tag{57}$$

for $n = 1, 2, 3, ..N_{Lobes}^{TSW}$. The results (54)–(57) hold for a single strip in the absence of a via. The presence of the trigonometric functions multiplying f_{sd} in (45)–(47) will modify the above angles somewhat.

2.2.3. Single Strip With Standing Wave Current

[19] If, instead of (19) we assume a general traveling wave–standing wave current,

$$J_z = I_0^s \delta(x) \frac{1}{\sqrt{1 - \left(\frac{y-y_0}{w}\right)^2}} T_n\left(\frac{y-y_0}{w}\right) \times \left(e^{-j\gamma_{ms}z} - \Gamma e^{j\gamma_{ms}z}\right), \tag{58}$$

for $|y - y_0| < w$ and $-L_1 < z < L_2$, where Γ is a reflection coefficient,

$$\Gamma = \Gamma_L e^{-j2\gamma_{ms}L_2}, \tag{59}$$

then (21), because of enforcement of current continuity, is replaced by

$$I_0^s = \frac{I_0^p}{w\pi\left(e^{-j\gamma_{ms}z_0} - \Gamma_L e^{-j2\gamma_{ms}L_2} e^{j\gamma_{ms}z_0}\right)}. \tag{60}$$

As with the previous case, we take $n = 0$ in (58). The results (45)–(47) are applicable, with f_{sd} (37) replaced by f_{sd}^{stw}, where

$$f_{sd}^{stw}(\beta_{sw}, \phi) = \left(\frac{\sin\left((\gamma_{ms} - \beta_{sw}\sin\phi)\frac{L}{2}\right)}{(\gamma_{ms} - \beta_{sw}\sin\phi)\frac{L}{2}} - \Gamma\frac{\sin\left((\gamma_{ms} + \beta_{sw}\sin\phi)\frac{L}{2}\right)}{(\gamma_{ms} + \beta_{sw}\sin\phi)\frac{L}{2}}\right) \cdot J_0(w\beta_{sw}\cos\phi). \tag{61}$$

2.2.4. Coupled Strips

[20] Assume that, instead of a single strip, we have two coupled strips as shown in Figure 3. If the strips are centered at $y = \pm y_0$, we have

$$J_{z1} = a_1\delta(x)\frac{1}{\sqrt{1 - \left(\frac{y+y_0}{w}\right)^2}} T_n\left(\frac{y+y_0}{w}\right) \times \left(e^{-j\gamma_{ms}z} - \Gamma_1 e^{j\gamma_{ms}z}\right) \tag{62}$$

$$J_{z2} = a_2\delta(x)\frac{1}{\sqrt{1 - \left(\frac{y-y_0}{w}\right)^2}} T_n\left(\frac{y-y_0}{w}\right) \times \left(e^{-j\gamma_{ms}z} - \Gamma_2 e^{j\gamma_{ms}z}\right) \tag{63}$$

for $|y \pm y_0| < w$ and $-L_1 < z < L_2$, where $\Gamma_{1,2}$ are the reflection coefficients at the load of the strips (each has

the form (59)) and we will again use $n = 0$. The resulting fields due to coupled strips are

$$E_x^{cs} = E_{0x}\left(a_1 \sin\phi_1 f_{sd}^{stw}(\beta_{sw},\phi_1)\frac{e^{-j\beta_{sw}\rho_s^{(1)}}}{\sqrt{\rho_s^{(1)}}} + a_2 \sin\phi_2 f_{sd}^{stw}(\beta_{sw},\phi_2)\frac{e^{-j\beta_{sw}\rho_s^{(2)}}}{\sqrt{\rho_s^{(2)}}}\right) \quad (64)$$

$$E_y^{cs} = E_{0y}\left(a_1 \sin\phi_1 \cos\phi_1 f_{sd}^{stw}(\beta_{sw},\phi_1)\frac{e^{-j\beta_{sw}\rho_s^{(1)}}}{\sqrt{\rho_s^{(1)}}} + a_2 \sin\phi_2 \cos\phi_2 f_{sd}^{stw}(\beta_{sw},\phi_2)\frac{e^{-j\beta_{sw}\rho_s^{(2)}}}{\sqrt{\rho_s^{(2)}}}\right) \quad (65)$$

$$E_z^{cs} = E_{0z}\left(a_1 \sin^2\phi_1 f_{sd}^{stw}(\beta_{sw},\phi_1)\frac{e^{-j\beta_{sw}\rho_s^{(1)}}}{\sqrt{\rho_s^{(1)}}} + a_2 \sin^2\phi_2 f_{sd}^{stw}(\beta_{sw},\phi_2)\frac{e^{-j\beta_{sw}\rho_s^{(2)}}}{\sqrt{\rho_s^{(2)}}}\right), \quad (66)$$

where

$$\rho_s^{(2,1)} = \sqrt{(y \mp y_0)^2 + z^2} \quad (67)$$

and

$$y - y_0 = \rho_s^{(2)}\cos\phi_2,\ z = \rho_s^{(2)}\sin\phi_2 \quad (68)$$

$$y + y_0 = \rho_s^{(1)}\cos\phi_1,\ z = \rho_s^{(1)}\sin\phi_1. \quad (69)$$

[21] For coupled strips (ignoring the vias) the beam maximum and minimum can be obtained numerically from (64)–(66), or from a simpler approximate expression as derived below. Using

$$\rho_s^{(2,1)} \simeq \rho\left(1 + \frac{y_0^2 \mp 2yy_0}{2\rho^2}\right),\quad \phi_1 \simeq \phi_2 \simeq \phi, \quad (70)$$

where $\rho = (y^2 + z^2)^{1/2}$, then, for example,

$$E_x^{cs} = E_{0x}\sin\phi f_{sd}^{stw}(\beta_{sw},\phi)\frac{e^{-j\beta_{sw}\rho}}{\sqrt{\rho}}e^{-j\beta_{sw}\frac{y_0^2}{2\rho}} \times \left(a_1 e^{-j\beta_{sw}y_0\cos\phi} + a_2 e^{j\beta_{sw}y_0\cos\phi}\right). \quad (71)$$

If $a_1 = -a_2 = -1$ (leading to the odd mode, which is the case of most interest for leakage on coupled strips), then

$$E_x^{cs} = 2jE_{0x}\frac{e^{-j\beta_{sw}\rho\left(1+\frac{y_0^2}{2\rho^2}\right)}}{\sqrt{\rho}}\sin\phi \times f_{sd}^{stw}(\beta_{sw},\phi)\sin(\beta y_0\cos(\phi)). \quad (72)$$

The presence of reflected waves is found to have a minor effect on beam angles (see section 3, and so, setting $\Gamma = 0$ in f_{sd}^{stw}, beam maxima and nulls for coupled strips can be found numerically from the relatively simple expression

$$BE(\phi) = \sin(\phi)\frac{\sin\left((\gamma - \beta\sin(\phi))\frac{L}{2}\right)}{(\gamma - \beta\sin(\phi))\frac{L}{2}}\sin(\beta y_0\cos(\phi)) \sim \sin(2\phi)\frac{\sin\left((\gamma - \beta\sin(\phi))\frac{L}{2}\right)}{(\gamma - \beta\sin(\phi))\frac{L}{2}}, \quad (73)$$

where the second expression is obtained assuming $\beta y_0 \ll 1$. Beam maxima obtained from a numerical search of (73) will be denoted as $\phi_{\max}^{BE}$, which obviously includes strip coupling but not the via fields (and holds in both the TSW and LW regimes). Comparing (73) and (53) it is clear that the number of beams for coupled strips in the TSW regime, and the angles for beam nulls, will be approximately the same as for single strips (the term $\sin(\beta y_0\cos(\phi))$ will not contribute additional beam nulls if βy_0 is reasonably small). Thus, for coupled strips,

$$N_{Lobes}^{TSW} \simeq \frac{L\beta_{ms}}{2\pi} \quad (74)$$

$$\phi_{null}^{TSW} \simeq \sin^{-1}\left(\frac{\beta_{ms}}{\beta_{sw}} \mp 2n\frac{\pi}{L\beta_{sw}}\right) \quad (75)$$

for $n = 1,2,3,..N_{Lobes}^{TSW}$. However, the angles of beam maxima will be somewhat different from (54) and (55). In particular, for sufficiently large L the sine function in (73) is rapidly varying compared to the term $\sin(2\phi)$, and thus (54) and (55) will hold approximately for sufficiently long coupled strips. For small L the sinc function is smoothly varying, and the function $\sin(2\phi)$ will play an important role in determining the beam maxima. The influence of strip length is further discussed in section 3.

[22] Note that mutual coupling effects are implicitly accounted for, since the full-wave complex propagation constant of two coupled strips is used in the asymptotic formula. The current profiles, (62) and (63), do not incorporate proximity effects (since only the dominant term of the current expansion in terms of Chebyshev polynomial is used), although it is well known that the far field of an antenna is somewhat insensitive to the

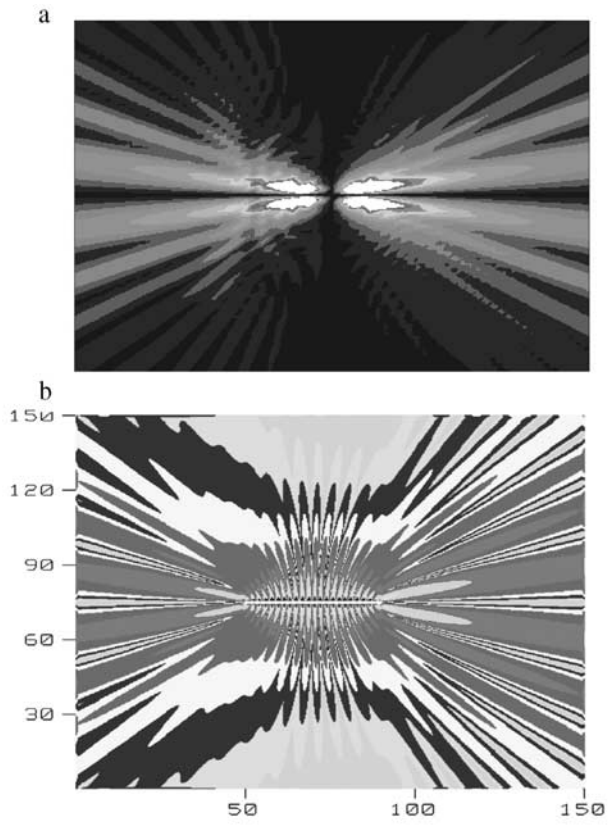

Figure 4. Vertical electric field at the air-dielectric interface ($x = 0$) due to two coupled via-fed interconnects, $\varepsilon_2 = 2.25\varepsilon_0$, $\varepsilon_3 = \varepsilon_0$, $d = 1$ cm, $L = 40$ cm, $w = 0.125$ cm, $b = 0.25$ cm (see Figure 3), and $f = 6.5$ GHz: (a) asymptotic formula and (b) full-wave simulation. The horizontal axis is z, and the vertical axis is y. See color version of this figure in the HTML.

antenna's current. Therefore the error due to neglecting the proximity effect in (62) and (63) is expected to be small.

2.2.5. Total Fields

[23] The field due to strip interconnects and vias is given by

$$\mathbf{E}(\mathbf{r}) = \mathbf{E}^s(\mathbf{r}) + \sum_{n=1}^{N_V} \mathbf{E}_n^v(\mathbf{r}), \tag{76}$$

where $\mathbf{E}^s$ is the field due to the strips, given by (45)–(47) for a single strip and (64)–(66) for coupled strips, N_V is the number of vias, and for each via $\mathbf{E}_n^v$ is given by (10)–(12). Beam maxima obtained from a numerical search of (76) will be denoted as $\phi_{\max}^{ASY}$.

3. Discussion and Results

[24] Before presenting results it is worthwhile to emphasize some differences between two- and three-dimensional transmission line/interconnect structures. In the usual two-dimensional transmission line theory leading to the generation of dispersion curves, one studies a source-free infinite structure. For perfectly conducting lines immersed in lossless dielectrics, this leads to the concept of bound modes characterized by real-valued propagation constants, and "leaky modes" characterized by complex-valued propagation constants. The bound modes do not radiate, but carry energy along the line. The leaky modes are not part of the proper spectrum of the integrated transmission line (i.e., their fields do not obey the usual radiation condition at infinity in certain directions normal to the line; the leaky mode field is exponentially growing in these directions), but can be useful as an approximation of the continuous spectrum of the structure in restricted areas of space. If radiation takes place, it is represented by the continuous spectrum, or its leaky mode approximation.

[25] For a three-dimensional interconnect the situation is quite different. An excitation such as a via may result in currents on the finite length transmission line section that resemble various bound and/or leaky modes corresponding to an infinite line, but with a different interpretation in terms of radiation. For example, on a finite-length transmission line a general current such as $I_0(e^{-j\beta z} - \Gamma e^{j\beta z})$, with $0 \leq |\Gamma| \leq 1$, will radiate energy into space and surface waves, even though β is real valued (e.g., consider a printed patch antenna, which typically has a standing wave current given by setting $\Gamma = 1$). This will be the case even if β is equal to a modal propagation constant on an infinite line. A traveling wave antenna [*Johnson*, 1993; *Stutzman and Thiele*, 1998] results from setting $\Gamma = 0$. We refer to this general situation as the traveling/standing wave (TSW) regime. For the printed interconnect in the TSW regime there will be $N_{Lobes}^{TSW} = L\beta_{ms}/2\pi$ (see (56) or (74)) forward lobes in the angular range $0 \leq \phi \leq 90°$ for a traveling wave antenna, and, in the event of a standing wave pattern, an equal number of backward lobes in the range $-90 \leq \phi \leq 0°$.

[26] If, however, the current on the line resembles a leaky wave current, then the beam angle should correspond to a leaky wave angle (β_{ms} represents a fast wave with respect to β_{sw}). If the leakage constant is sufficiently large, in the leaky wave regime there will be one forward lobe in the angular range $0 \leq \phi \leq 90°$ ($N_{Lobes}^{LW} = 1$). This is a principal difference between the TSW and LW regimes on a three-dimensional interconnect; in the former $\gamma_{ms} \simeq \beta_{ms} > \beta_{sw}$ ($\alpha_{ms} \ll 1$), resulting in a multilobe pattern, and in the latter, α_{ms} becomes larger, resulting in essentially single-lobe radiation.

[27] Furthermore, on an infinite two-dimensional structure the leakage field increases exponentially in the leakage direction, and on a source-excited infinite or semi-infinite line the leakage field increases up to a point

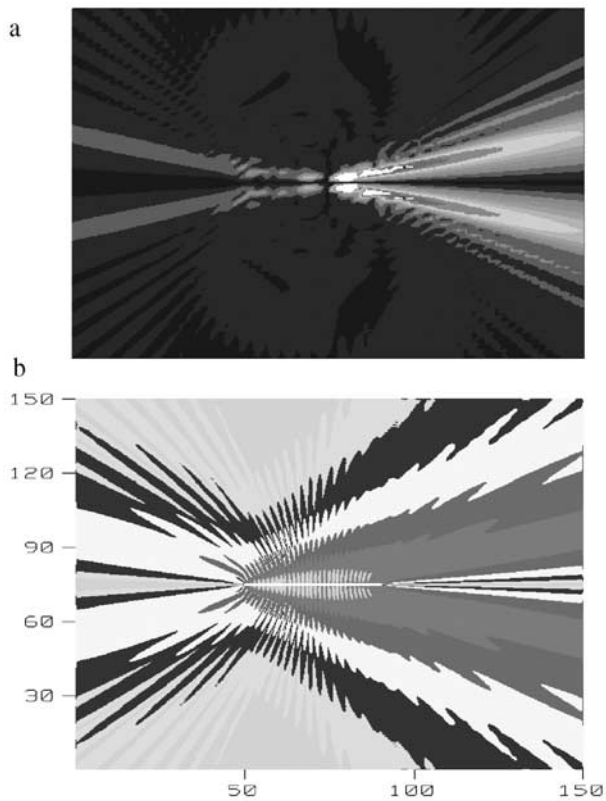

Figure 5. Same as Figure 4 except that f = 9 GHz. See color version of this figure in the HTML.

called the leakage boundary [*Villegas et al.*, 1999]. On a three-dimensional line, radiation into a surface wave will be in the form of beams or lobes, regardless of whether the current is a standing wave (such as when $|\Gamma| = 1$), a traveling wave (as in a conventional traveling wave antenna), or a leaky wave. In this study TSW and leaky wave excitation will be identified by the correspondence between the predicted and observed number of lobes, and angle of maximum radiation.

[28] A plot of normalized E_x (vertical electric field) is shown in Figures 4, 5, 6, 7, 8, and 9 for two coupled microstrip interconnects on a grounded slab having dielectric constant $\varepsilon_2 = 2.25\varepsilon_0$, $\varepsilon_3 = \varepsilon_0$, and dielectric thickness d = 1 cm (see Figure 3). Coupled interconnects are considered since the odd mode becomes leaky above a certain frequency [see, e.g., *Shigesawa et al.*, 1995; *Yakovlev and Hanson*, 1997], and hence one can examine field behavior in what should be (via two-dimensional predictions) leaky and nonleaky regimes. The interconnects are perfectly conducting, and have width 0.25 cm and center-to-center separation 0.5 cm. Each interconnect is fed by a via on one end and open circuited at the other end. In Figures 4–6 long interconnects are considered, L = 40 cm (as an aid in comparing with two-dimensional leaky wave theory), and in Figures 7–9 shorter interconnects are considered, L = 5 cm. In each figure the computational space is 150 × 150 cm^2, and the interconnects are located in the center of the computation area.

[29] In Figures 4–9, part a shows the closed-form analytical result (76), which is the sum of the fields due to two vias (each carrying opposing ±1 A currents so as to excite the odd strip mode), given by two terms of the form (10), and horizontal strip fields given by (64) using $a_1 = I_0^s$, $a_2 = -I_0^s$. Since the load end of the strips are open circuited, we assume $\Gamma_L = 1$ in the reflection coefficients for each strip. The angle of maximum radiation for the asymptotic result, $\phi_{\max}^{ASY}$, was obtained by numerical root search of the total field (76), then rounded to the nearest degree. In part b the field E_x obtained by full-wave (FW) simulation (Ansoft Ensemble) is shown. For the full-wave result the radiation angle $\phi_{\max}^{FW}$ was obtained from the plot. In obtaining radiation angles from the plots, errors of several degrees can be expected, primarily due to ambiguity in locating the beam peak. Plot legends are not included since the asymptotic

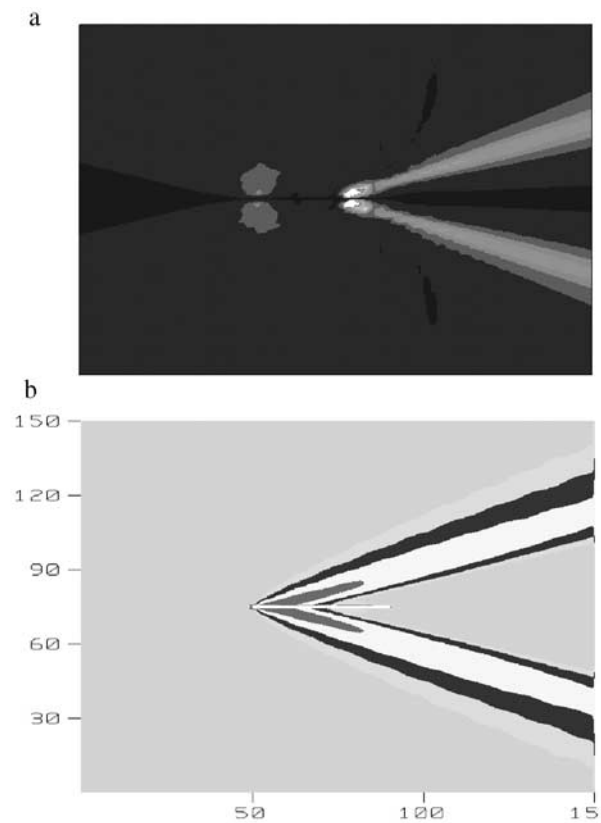

Figure 6. Same as Figure 4 except that f = 13 GHz. See color version of this figure in the HTML.

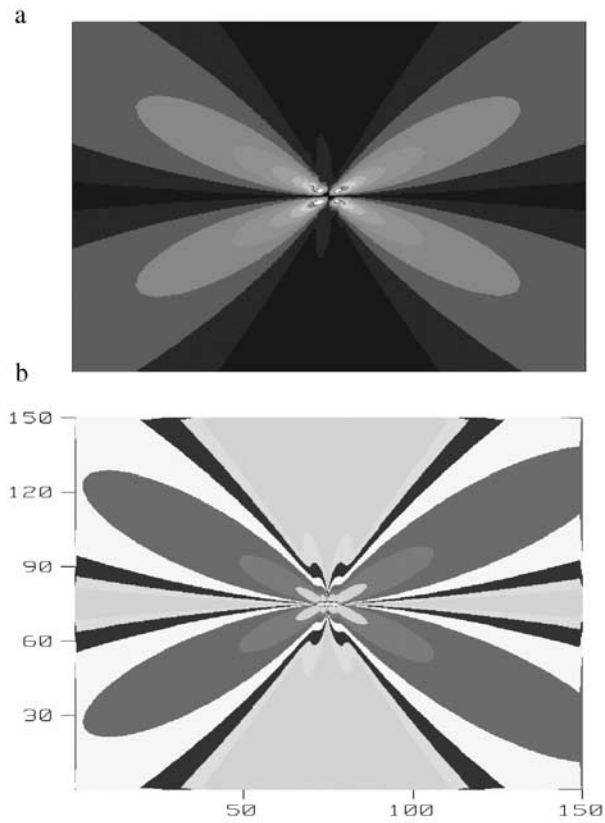

Figure 7. Vertical electric field at the air-dielectric interface ($x = 0$) due to two coupled via-fed interconnects, $\varepsilon_2 = 2.25\varepsilon_0$, $\varepsilon_3 = \varepsilon_0$, $d = 1$ cm, $L = 5$ cm, $w = 0.125$ cm, $b = 0.25$ cm (see Figure 3), and $f = 6.5$ GHz: (a) asymptotic formula and (b) full-wave simulation. The horizontal axis is z, and the vertical axis is y. See color version of this figure in the HTML.

result assumes ±1 A on each via, and the full-wave result places ±1 volt at the base of each via, and so numerical comparison of the field amplitudes is not possible.

[30] The full-wave dispersion curves for the infinite-length coupled microstrip transmission line case are shown in Figure 1 of *Yakovlev and Hanson* [1997], from which the propagation constant values utilized below were obtained. From these plots it is evident that for $f \lesssim 8$ GHz the odd mode is bound, whereas above 8 GHz the odd mode is leaky. In this study we consider three frequencies, $f = 6.5$ GHz (bound regime), $f = 9$ GHz, and 13 GHz (leaky regime).

[31] The case of a very long interconnect ($L = 40$ cm) is considered in Figures 4–6. In Figure 4 the frequency of operation is 6.5 GHz, at which point the odd mode propagation constant on an infinite pair of strips is $\gamma_{ms} \simeq 1.29k_0$, whereas $\beta_{sw} \simeq 1.25k_0$. Since $\beta_{ms} > \beta_{sw}$ we would expect that the mode is not leaky. The vertical electric field at the air-dielectric surface shows a fairly symmetric pattern, consistent with standing current waves, and does not seem to exhibit classical leakage. Radiation exists, in the same way that a printed patch antenna or strip dipole antenna radiates into space and surface waves. The number of radiation lobes predicted by the traveling/standing wave theory (74) is $N_{Lobes}^{TSW} = 11$, which is the same number observed in the full-wave and asymptotic plots (although in the asymptotic plots some lobes are difficult to see because of plot contrast). It is clear that the traveling/standing wave theory accounts for the observed field behavior.

[32] In Figure 5 the frequency of operation is 9 GHz, where $\gamma_{ms} \simeq (1.31 - j0.019)\, k_0$ and $\beta_{sw} \simeq 1.34k_0$, and, since $\Re\{\gamma_{ms}\} < \beta_{sw}$, one expects the mode to be leaky. The asymptotic result predicts a leakage angle of $\phi_{\max}^{ASY} \simeq 74°$, which agrees with the full-wave result, and the two-dimensional single strip leakage angle is $\phi_{\max}^{LW,2D} = 77°$ from (54). The number of observed radiation lobes ($N_{Lobes}^{FW} \simeq 16$) is the same as the value predicted by the traveling/standing wave theory. Thus, although the leakage angle is close to the observed radiation angle, the presence of multiple lobes, close to the TSW prediction,

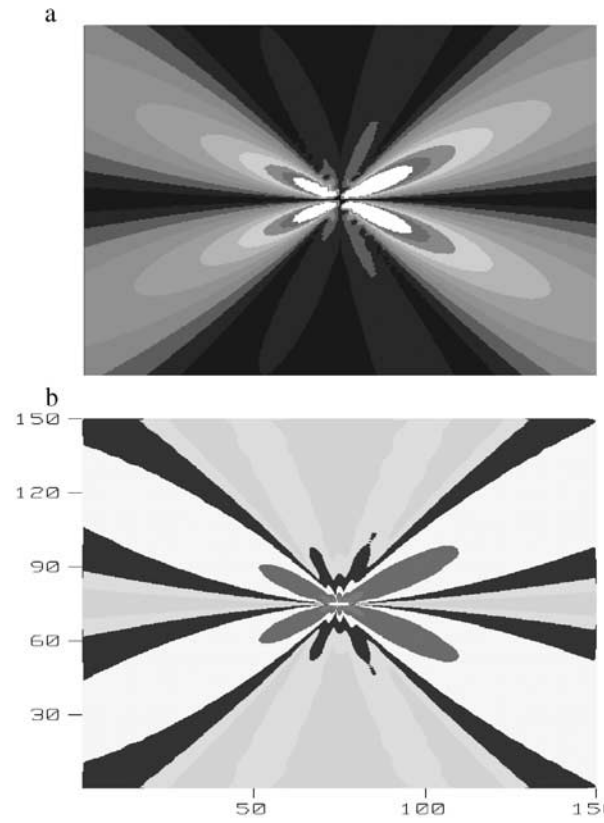

Figure 8. Same as Figure 7 except that $f = 9$ GHz. See color version of this figure in the HTML.

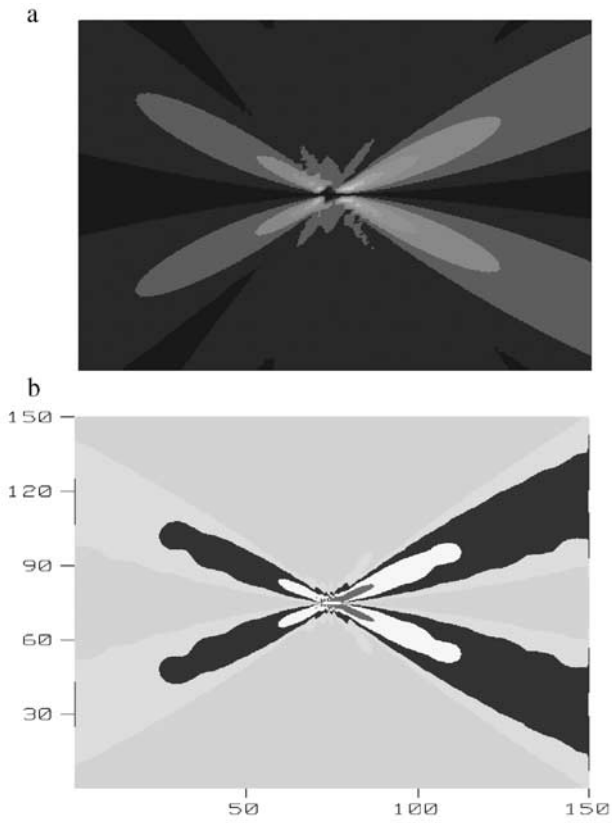

Figure 9. Same as Figure 7 except that $f = 13$ GHz. See color version of this figure in the HTML.

indicates that the TSW theory seems to account for the interconnect radiation. However, it seems that leakage is starting to emerge.

[33] In Figure 6, results are shown for $f = 13$ GHz, in which case $\gamma_{ms} \simeq (1.30 - j0.03)\, k_0$ and $\beta_{sw} \simeq 1.42 k_0$. Therefore, on the basis of propagation constant values one expects the mode to be leaky. The radiation angle predicted by the asymptotic theory is $\phi_{\max}^{ASY} \simeq 67°$, which is approximately the same angle obtained from the full-wave plot, and, also, $\phi_{\max}^{LW,2D} = 67°$. In this case one lobe is observed, which, together with the correspondence between the beam angles, indicates that a leaky wave is providing the dominant effect.

[34] Results are summarized in Table 1. Note that the angle $\phi_{\max}^{ASY}$, arising from (76), accounts for via excitation, whereas $\phi_{\max}^{BE}$, arising from (73), assumes close strip spacing and ignores the via excitation. For the $L = 40$ cm case they provide the same result.

[35] In Figures 7–9 coupled interconnects having $L = 5$ cm are considered at $f = 6.5$ GHz, 9 GHz, and 13 GHz, respectively. Generally, the above described conclusions for the $L = 40$ cm interconnect seem to apply to the $L = 5$ cm interconnect, and results are summarized in Table 2. However, unlike the $L = 40$ cm case, upon comparing $\phi_{\max}^{ASY}$ and $\phi_{\max}^{BE}$ it can be seen that for the $L = 5$ cm interconnects the presence of the via has some influence on the beam angle. Results at other frequencies yielded good agreement as well, but will be omitted because of space limitations. In all cases the asymptotic theory agrees well with the full-wave results, in both the TSW and LW regimes.

Table 1. Radiation Parameters for $L = 40$ cm Interconnect[a]

f, GHz	N_{Lobes}^{TSW}	N_{Lobes}^{FW}	$\phi_{\max}^{FW}$, deg	$\phi_{\max}^{ASY/BE}$, deg	$\phi_{\max}^{LW,2D}$, deg
6.5	11	11	79	79/79	–
9.0	16	16	74	74/74	77
13	–	1	67	67/67	67

[a]The superscripts *TSW*, *FW*, *ASY*, and *LW* indicate the traveling/standing wave theory, the full-wave results, the asymptotic results, and the two-dimensional leaky wave angle (54) (for a single strip), respectively. If more than one radiation maximum occurs, the angle $\phi_{\max}$ refers to the main lobe.

[36] The influence of reflected waves was also more important on the shorter interconnect. If, in the asymptotic model, $\Gamma = 0$ was used, the radiation angle changed approximately one degree for the $L = 5$ cm interconnect, although there was no change for the $L = 40$ cm interconnect.

[37] Of more importance, at least for shorter interconnects, is strip coupling (as explained in the text after (73)). For example, at $f = 13$ GHz the $L = 5$ cm ($L \simeq 2.1\lambda_0$) coupled interconnects leak at $\phi_{\max}^{FW} \simeq 56°$, and the $L = 40$ cm ($L \simeq 17.3\lambda_0$) interconnects leak at $\phi_{\max}^{FW} \simeq 67°$, which is also the two-dimensional, single strip leakage angle. For small L the observed difference in leakage angles is explained by the presence of two strips, as indicated by a careful consideration of (73). As further confirmation of this, we simply removed one strip and via from the asymptotic model, leading to a single strip (*SS*) and via (keeping the same value of γ_{ms} as for the coupled strips). The result was that for the $L = 40$ cm interconnect the leakage angle was 67° for both the single and coupled strip cases. However, for the $L = 5$ cm interconnect the leakage angles were different, with the single strip case leakage angle close to the simple two-dimensional result, as shown in Table 3. The ability to include or not include various factors such as the via

Table 2. Radiation Parameters for $L = 5$ cm Interconnect[a]

f, GHz	N_{Lobes}^{TSW}	N_{Lobes}^{FW}	$\phi_{\max}^{FW}$, deg	$\phi_{\max}^{ASY/BE}$, deg
6.5	1	1	53	54/56
9.0	2	2	56	56/58
13	–	1	56	56/59

[a]The superscripts *TSW*, *FW*, and *ASY* indicate the traveling/standing wave theory, the full-wave results, and the asymptotic results, respectively. If more than one radiation maximum occurs, the angle $\phi_{\max}$ refers to the main lobe.

Table 3. Influence of the Presence of Coupled Versus Single Strips on Leakage Angle (Keeping the Propagation Constant γ_{ms} Constant)[a]

	L = 5 cm	L = 40 cm
f, GHz	13	13
$\phi_{\max}^{ASY,CS}$, deg	56	67
$\phi_{\max}^{ASY,SS}$, deg	65	67

[a]The superscripts *CS* and *SS* indicate coupled and single strips, respectively.

excitation, reflections, and strip coupling is one reason the asymptotic development is particularly useful.

[38] In Figure 10 the magnitude of the vertical electric field versus position z (i.e., parallel to the interconnect), at three distances perpendicularly away from two coupled long interconnects (y = 10, 25, 40 cm) is shown at 13 GHz (I_0^p = 1 A). The geometry is the same as in Figure 6 (L = 40 cm), and the field shown in Figure 10 is simply a horizontal cut from Figure 6a. Results are calculated from the asymptotic formula, and the presence of a strong leakage beam is evident. Figure 11 shows the same result for L = 5 cm interconnects (the field shown is simply a horizontal cut from Figure 9a). It can be appreciated that the field is stronger for the longer interconnects, since they have sufficient length for a strong leakage beam to build up.

[39] On the basis of results of the asymptotic theory, verified by full-wave simulation, the following observations can be made.

[40] 1. At frequencies well below and well above the onset of surface wave leakage on two-dimensional structures (f = 6.5 GHz and 13 GHz, respectively for the structure considered here, with $f \simeq 8$ GHz being the leakage cutoff point), the presence or absence of leakage into surface waves on finite via-fed interconnects did seem to correspond with the regimes predicted by two-dimensional theory. Closer to the leakage cutoff point the situation is less clear; however, no attempt was made in this study to examine the emergence of leakage as a function of frequency.

[41] 2. On a finite-length interconnect with a nonideal load termination, the presence of reflected current waves seems to merely produce backward radiation beams, in both the traveling/standing wave and leaky wave regimes (as might be expected).

[42] 3. On relatively long coupled interconnects the leakage angle is well predicted by simple two-dimensional ray optic theory, although on shorter interconnects the interconnect length L plays a significant role in determining the leakage angle, mainly due to strip coupling, but also to the interaction between the via and strip fields, and to the presence of reflected waves.

4. Conclusion

[43] Leaky wave effects on three-dimensional microstrip via-fed interconnects have been considered. An asymptotic formulation has been developed to model

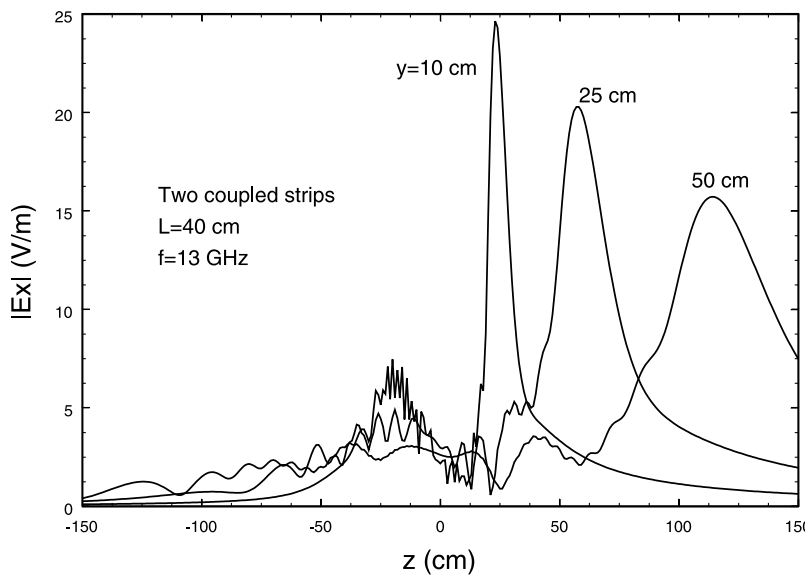

Figure 10. Magnitude of the vertical electric field versus position z (parallel to the interconnect), at three distances perpendicularly away from two coupled long interconnects (y = 10, 25, and 40 cm). Frequency is 13 GHz, I_0^p = 1 A, and the geometry is the same as in Figure 6 (L = 40 cm).

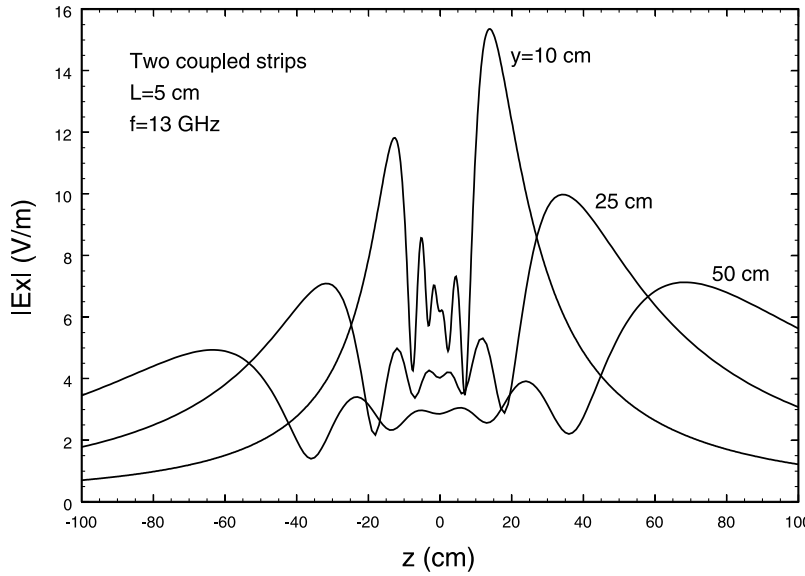

Figure 11. Magnitude of the vertical electric field versus position z (parallel to the interconnect), at three distances perpendicularly away from two coupled long interconnects (y = 10, 25, and 40 cm). Frequency is 13 GHz, I_0^p = 1 A, and the geometry is the same as in Figure 9 (L = 5 cm).

the radiation fields, accounting for both the via feeds and horizontal strip currents. Comparison to full-wave numerical simulation was used to verify the formulation. The asymptotic formulation requires knowledge of the propagation constant on an infinite (two-dimensional) microstrip transmission line, but yields closed-form expressions which accurately predict the fields due to traveling/standing waves and leaky waves on the interconnect, including the via fields. The influence of strip length and mismatched load terminations have been discussed.

Appendix A: Continuous Spectrum Contribution

[44] In this appendix we show that along the air-dielectric interface the continuous spectrum contribution varies as $1/\rho^2$ in the far field, and hence can be ignored compared to the discrete contribution.

[45] A generic continuous spectrum contribution is given in (2) as

$$\chi = \int_0^\infty \mathbf{u}_\kappa^{\beta\beta}(x)\,\overline{v}_{\kappa,\beta\beta}(x')H_0^{(2)}\left(\sqrt{k_u^2-\kappa}\rho\right)d\kappa. \quad \text{(A1)}$$

For demonstration purposes we concentrate on the TM continuous spectrum component $\chi_{xx}^{(3)}$ where the superscript indicates that the spectrum is evaluated in region 3 (actually at the air-dielectric interface). In this case, using (75), (81), and (83) from *Hanson* [2005] we obtain

$$\chi_{xx}^{(3)}(0) = \frac{N^4}{4\pi j} \cdot \int_0^\infty \frac{\sqrt{\kappa}H_0^{(2)}\left(k_0\rho\sqrt{1-\kappa/k_0^2}\right)}{\left(\kappa-k_0^2+k_2^2\tan^2\sqrt{\kappa-k_0^2+k_2^2}d+N^4\kappa\right)}d\kappa. \quad \text{(A2)}$$

Replacing the Hankel function with its large-argument form leads to

$$\chi^{(3)}(0) = \frac{N^4}{4\pi j}\sqrt{\frac{2}{\pi k_0\rho}}e^{j\pi/4}\int_0^\infty K(\kappa)\sqrt{\kappa}e^{-jk_0\rho\sqrt{1-\kappa/k_0^2}}d\kappa, \quad \text{(A3)}$$

where

$$K(\kappa) = \frac{1}{\left(\left(\kappa-k_0^2+k_2^2\right)\tan^2\left(\sqrt{\kappa-k_0^2+k_2^2}d\right)+N^4\kappa\right)} \times \frac{1}{\left(1-\kappa/k_0^2\right)^{1/4}}. \quad \text{(A4)}$$

Taking the first term of power series expansion of $K(\kappa)$ about $\kappa = 0$ and making the approximation

$$\sqrt{1-\frac{\kappa}{k_0^2}} \simeq 1-\frac{\kappa}{2k_0^2} \quad \text{(A5)}$$

for $\kappa/k_0^2 \ll 1$ leads to

$$\chi^{(3)}(0) \simeq \sqrt{\frac{2}{\pi k_0 \rho}} \frac{N^4 e^{j\pi/4} e^{-jk_0\rho}}{4\pi j\left(\left(k_2^2 - k_0^2\right)\tan^2\left(\sqrt{k_2^2 - k_0^2}d\right)\right)} \times \int_0^\infty \sqrt{\kappa} e^{j\frac{\rho}{2k_0}\kappa} d\kappa. \quad \text{(A6)}$$

The integral can be approximated using the Watson transform,

$$\int_0^\infty s^a e^{-s\Delta} ds = \frac{\Gamma(a+1)}{\Delta^{a+1}}, \quad \text{(A7)}$$

which holds for Δ complex, $|\Delta| \to \infty$, with arg $(\Delta) < \pi/2$ [*Bleistein and Handelsman*, 1975] to yield

$$\chi^{(3)}(0) = \frac{jk_0 N^4 \Gamma(3/2)}{\pi^{3/2}\left(\left(k_2^2 - k_0^2\right)\tan^2\left(\sqrt{k_2^2 - k_0^2}d\right)\right)} \frac{e^{-jk_0\rho}}{\rho^2}, \quad \text{(A8)}$$

where Γ is the gamma function (Γ (3/2) $\simeq$ 0.886). The asymptotic result (A8) was compared to a numerical integration of (A2), and agreement was seen to be very good. Therefore, along the surface of the air-dielectric interface for $\rho \gg 1$, the continuous spectrum varies as $1/\rho^2$, and hence is not important compared to the discrete spectrum contribution (that varies as $1/\rho^{1/2}$).

Appendix B: Semi-Infinite Interconnect

[46] In this appendix we consider the case of a semi-infinite strip, and show that the dominant leakage field is due to a residue contribution, instead of a saddle-point contribution as was the case for a finite interconnect. Assume $L_1 = 0$, $L_2 \to \infty$. In this case

$$I_{SD} = \int_{SDP} g^{si}(\theta) e^{-j\beta_{sw}\rho\cos(\theta-\phi)} d\theta + R, \quad \text{(B1)}$$

where

$$g^{si}(\theta) = \pi^2 w \frac{J_0(\beta_{sw} w \cos\theta)}{(\gamma_{ms} - \beta_{sw}\sin\theta)} \quad \text{(B2)}$$

for $\gamma_{ms} = \beta_{ms} - j\alpha$, $\alpha > 0$. Therefore a pole exists in the steepest descent plane at

$$\theta_p = \sin^{-1}\frac{\gamma_{ms}}{\beta_{sw}}. \quad \text{(B3)}$$

In this case,

$$I_{SD} \simeq -g^{si}(\theta_s)\sqrt{2\pi}\frac{e^{-j\beta_{sw}\rho}}{\sqrt{\beta_{sw}\rho}} e^{j\pi/4} + H(\theta - \theta_p)R, \quad \text{(B4)}$$

where R is the captured residue and $H(\theta)$ is the Heaviside function. With $\theta_s = \phi$,

$$I_{SD}(\phi,\rho) = -\pi^2 w e^{j\pi/4}\sqrt{2\pi}\frac{J_0(\beta_{sw}\cos\phi w)}{(\gamma_{ms} - \beta_{sw}\sin\phi)}\frac{e^{-j\beta_{sw}\rho}}{\sqrt{\beta_{sw}\rho}} + H(\theta - \theta_p)R. \quad \text{(B5)}$$

Assume $\alpha \ll \beta_{ms}$. Then, if $\beta_{ms} > \beta_{sw}$,

$$\theta_p = \pm\left(\frac{\pi}{2} - j\delta\right),\ \delta > 0 \quad \text{(B6)}$$

and the pole is not encountered when C is deformed to the steepest descent path (see Figure 2), unless δ is sufficiently small.

[47] If $\beta_{ms} < \beta_{sw}$ then θ_p occurs on the real θ axis, $-\pi/2 < \theta_p < \pi/2$ (actually just below the real axis for $0 < \alpha \ll 1$), and the pole will be encountered when C is deformed to the steepest descent path, beginning approximately when $\phi = \theta_s = \theta_p$).

[48] For $\phi \geq \theta_p$ the residue contribution is

$$R = (2\pi i)\pi^2 w \frac{J_0(\beta_{sw}\cos\theta_p w)}{\frac{d}{d\theta}(\gamma_{ms} - \beta_{sw}\sin\theta)\big|_{\theta_p}} e^{-j\beta_{sw}\rho\cos(\theta_p - \phi)} = -(2\pi i)\pi^2 w \frac{J_0(\beta_{sw}\cos\theta_p w)}{(\cos\theta_p)\beta_{sw}} e^{-j\beta_{sw}\rho\cos(\theta_p - \phi)}. \quad \text{(B7)}$$

Therefore

$$I_{SD}(\phi,\rho) = -\pi^2 w\left(e^{j\pi/4}\sqrt{2\pi}\frac{J_0(\beta_{sw} w\cos\phi)}{(\gamma_{ms} - \beta_{sw}\sin\phi)}\frac{e^{-j\beta_{sw}\rho}}{\sqrt{\beta_{sw}\rho}} + (2\pi i)\frac{J_0(\beta_{sw} w\cos\theta_p)}{(\cos\theta_p)\beta_{sw}} e^{-j\beta_{sw}\rho\cos(\theta_p - \phi)}\right). \quad \text{(B8)}$$

Assuming ϕ is not at the shadow boundary, then the second term (residue contribution) dominates for $\rho \gg 1$, leading to

$$I_{SD}(\phi,\rho) \simeq -\pi^2 w(2\pi i)\frac{J_0(\beta_{sw} w\cos\theta_p)}{(\cos\theta_p)\beta_{sw}} e^{-j\beta_{sw}\rho\cos(\theta_p - \phi)}. \quad \text{(B9)}$$

With

$$\cos\theta_p = \sqrt{1 - \left(\frac{\beta_{ms} - j\alpha_{ms}}{\beta_{sw}}\right)^2} \simeq \left(1 - \frac{1}{\beta_{sw}^2}\beta_{ms}^2 + \frac{j}{\beta_{sw}^2}\beta_{ms}\alpha_{ms}\right) \quad \text{(B10)}$$

$$\sin\theta_p = \frac{\gamma_{ms}}{\beta_{sw}} = \frac{\beta_{ms} - j\alpha_{ms}}{\beta_{sw}}$$

and

$$e^{-j\beta_{sw}\rho\cos(\theta_p-\phi)} = e^{-j\beta_{sw}\rho(\cos\theta_p\cos\phi+\sin\theta_p\sin\phi)} \simeq e^{-j\beta_{sw}y\left(1-\frac{1}{2\beta_{sw}^2}\beta_{ms}^2\right)} e^{y\frac{\beta_{ms}}{\beta_{sw}}\alpha_{ms}} e^{-jz(\beta_{ms}-j\alpha_{ms})}, \tag{B11}$$

then

$$\left|e^{-j\beta_{sw}\rho\cos(\theta_p-\phi)}\right| \simeq e^{-\alpha_{ms}z} e^{\frac{\beta_{ms}}{\beta_{sw}}\alpha_{ms}y} \tag{B12}$$

indicates a wave exponentially increasing transverse to the strip (and exhibits the same behavior as (10) of *Villegas et al.* [1999], derived for a semi-infinite strip using a different method), which is the usual two-dimensional leaky wave behavior.

References

Bagby, J. S., C. L. Lee, D. P. Nyquist, and Y. Yuan (1993), Identification of propagation regimes on integrated microstrip transmission lines, *IEEE Trans. Microwave Theory Tech.*, *41*, 1887–1893.

Bleistein, N., and R. A. Handelsman (1975), *Asymptotic Expansions of Integrals*, Holt, Rinehart, and Winston, Austin, Tex.

Carin, L., and N. K. Das (1992), Leaky waves on broadside-coupled microstrip, *IEEE Trans. Microwave Theory Tech.*, *40*, 58–66.

Carin, L., G. W. Slade, and K. J. Webb (1998), Mode coupling and leakage effects in finite-size printed interconnects, *IEEE Trans. Microwave Theory Tech.*, *46*, 450–457.

Das, N. K. (1996), Power leakage, characteristic impedance, and leakage-transition behavior of finite-length stub sections of leaky printed transmission lines, *IEEE Trans. Microwave Theory Tech.*, *44*, 526–536.

Hanson, G. W. (2005), Dyadic Green's function for planar media—A dyadic eigenfunction approach, *IEEE Trans. Antennas Propag.*, *52*, 3350–3356.

Hanson, G. W., and A. B. Yakovlev (2004), Leaky wave excitation on three-dimensional printed interconnects, paper presented at 2004 International Microwave Symposium, Inst. Electr. and Electron. Eng., Fort Worth, Tex., 6–11 June.

Hanson, G. W., A. B. Yakovlev, and W. E. Hutchcraft (2004), Leaky wave excitation on three-dimensional printed interconnects, paper presented at 2004 International Symposium on Electromagnetic Theory, Union Radio Sci. Int., Pisa, Italy.

Jackson, D. R., F. Mesa, M. Freire, D. P. Nyquist, and C. Di Nallo (2000), An excitation theory for bound modes, leaky modes, and residual-wave currents on stripline structures, *Radio Sci.*, *35*, 495–510.

Johnson, R. C. (1993), *Antenna Engineering Handbook*, McGraw-Hill, New York.

Langston, W. L., J. T. Williams, D. R. Jackson, and F. Mesa (2003), Fundamental properties of radiation from a leaky mode excited on a planar transmission line, *IEEE Trans. Microwave Theory Tech.*, *51*, 2366–2377.

Mesa, F., and D. R. Jackson (2002), The danger of high-frequency spurious effects on wide microstrip line, *IEEE Trans. Microwave Theory Tech.*, *50*, 2679–2689.

Mesa, F., C. Di Nallo, and D. R. Jackson (1999), The theory of surface-wave and space-wave leaky-mode excitation on microstrip lines, *IEEE Trans. Microwave Theory Tech.*, *47*, 207–215.

Mesa, F., D. R. Jackson, and M. J. Freire (2001), High-frequency leaky-mode excitation on a microstrip line, *IEEE Trans. Microwave Theory Tech.*, *49*, 2206–2214.

Michalski, K. A., and D. Zheng (1989), On the leaky modes of open microstrip lines, *Microwave Opt. Technol. Lett.*, *2*, 6–8.

Nghiem, D., J. T. Williams, D. R. Jackson, and A. A. Oliner (1995), Leakage of the dominant mode on stripline with a small air gap, *IEEE Trans. Microwave Theory Tech.*, *43*, 2549–2556.

Nghiem, D., J. T. Williams, D. R. Jackson, and A. A. Oliner (1996), Existence of a leaky dominant mode on microstrip line with an isotropic substrate: Theory and measurements, *IEEE Trans. Microwave Theory Tech.*, *44*, 1710–1715.

Niu, D. C., T. Yoneyama, and T. Itoh (1993), Analysis and measurement of NRD-guide leaky wave coupler in Ka band, *IEEE Trans. Microwave Theory Tech.*, *41*, 2126–2132.

Nyquist, D. P., J. M. Grimm, D. J. Infante, and H. Braunisch (1997), Classification of the proper propagation-mode spectrum and leaky-wave modes on open planar waveguides, *Electromagnetics*, *17*, 105–130.

Shigesawa, H., M. Tsuji, and A. A. Oliner (1991), Dominant mode power leakage from printed-circuit waveguides, *Radio Sci.*, *26*, 559–564.

Shigesawa, H., M. Tsuji, and A. A. Oliner (1995), Simultaneous propagation of bound and leaky dominant modes on printed-circuit lines: A new general effect, *IEEE Trans. Microwave Theory Tech.*, *43*, 3007–3019.

Shigesawa, H., M. Tsuji, and A. A. Oliner (1996), New improper real and complex solutions for printed-circuit transmission lines and their influence on physical effects, *Radio Sci.*, *31*, 1639–1649.

Stutzman, W. L., and G. A. Thiele (1998), *Antenna Theory and Design*, 2nd ed., John Wiley, Hoboken, N. J.

Villegas, F. J., D. R. Jackson, J. T. Williams, and A. A. Oliner (1999), Leakage fields from planar semi-infinite transmission lines, *IEEE Trans. Microwave Theory Tech.*, *47*, 443–454.

Yakovlev, A. B., and G. W. Hanson (1997), On the nature of critical points in leakage regimes of a conductor-backed coplanar strip line, *IEEE Trans. Microwave Theory Tech.*, *45*, 87–94.

G. W. Hanson, Department of Electrical Engineering, University of Wisconsin-Milwaukee, 3200 N. Cramer Street, Milwaukee, WI 53211, USA.

W. E. Hutchcraft and A. B. Yakovlev, Department of Electrical Engineering, University of Mississippi, University, MS 38677, USA. (yakovlev@olemiss.edu)